

Biomedical Materials



PAPER

Multifunctional calcium phosphate based coatings on titanium implants with integrated trace elements

OPEN ACCESS

RECEIVED
15 July 2019

REVISED
22 November 2019


ACCEPTED FOR PUBLICATION
29 November 2019

PUBLISHED
27 February 2020

Original content from this work may be used under the terms of the [Creative Commons Attribution 3.0 licence](#).

Any further distribution of this work must maintain attribution to the author(s) and the title of the work, journal citation and DOI.



C Wolf-Brandstetter¹ , R Beutner¹, R Hess¹, S Bierbaum^{1,2}, K Wagner¹, D Scharnweber¹, U Gbureck³ and C Moseke⁴

¹ Max Bergmann Center of Biomaterials, Technische Universität Dresden, Dresden, Germany

² International Medical College, Schorlemerstr. 21, 48143 Münster, Germany

³ Department for Functional Materials in Medicine and Dentistry, University of Würzburg, Germany

⁴ Institute for Biomedical Engineering, University of Applied Sciences Gießen, Germany

E-mail: Cornelia.Wolf-Brandstetter@tu-dresden.de

Keywords: coating, titanium, implant, pro-angiogenic, osteogenic, antimicrobial

Supplementary material for this article is available [online](#)

Abstract

For decades, the main focus of titanium implants developed to restore bone functionality was on improved osseointegration. Additional antimicrobial properties have now become desirable, due to the risk that rising antibiotic resistance poses for implant-associated infections. To this end, the trace elements of copper and zinc were integrated into calcium phosphate based coatings by electrochemically assisted deposition. In addition to their antimicrobial activity, zinc is reported to attract bone progenitor cells through chemotaxis and thus increase osteogenic differentiation, and copper to stimulate angiogenesis. Quantities of up to $68.9 \pm 0.1 \mu\text{g cm}^{-2}$ of copper and $56.6 \pm 0.4 \mu\text{g cm}^{-2}$ of zinc were deposited; co-deposition of both ions did not influence the amount of zinc but slightly increased the amount of copper in the coatings. The release of deposited copper and zinc species was negligible in serum-free simulated body fluid. In protein-containing solutions, a burst release of up to $10 \mu\text{g ml}^{-1}$ was observed for copper, while zinc was released continuously for up to 14 days. The presence of zinc was beneficial for adhesion and growth of human mesenchymal stromal cells in a concentration-dependent manner, but cytotoxic effects were already visible for coatings with an intermediate copper content. However, co-deposited zinc could somewhat alleviate the adverse effects of copper. Antimicrobial tests with *E. coli* revealed a decrease in adherent bacteria on brushite without copper or zinc of 60%, but if the coating contained both ions there was almost no bacterial adhesion after 12 h. Coatings with high zinc content and intermediate copper content had the overall best multifunctional properties.

1. Introduction

Implants for bone substitution such as total hip implants and dental implants are frequently made from titanium. Despite their comparatively high success rates, their performance would benefit from improvements in the following areas: (i) shortening the initial healing period, (ii) enhancing osseointegration for patients with poor bone quality or who suffer from systemic diseases such as osteoporosis or diabetes, and (iii) lowering the risk of implant-associated infections—a matter of increasing importance, given the mounting prevalence of multiresistant microbes.

For several decades, the focus in implant development was solely on the promotion of osseointegration, but ideally, state-of-the-art implants should combine pro-osteogenic and antimicrobial properties [1]. To combat bacteria in acute infections, the use of antibiotics is still the method of choice. This is usually realized by systemic administration or local placement of antibiotics-releasing spacers. Recently, a variety of studies focused on the development of coatings for the local release of gentamicin [2] or vancomycin [3] for acute as well as prophylactic application. The main challenge in the local delivery of antibiotics is to release them for a sufficient time and with an effective dose

while avoiding a release below the minimal inhibitory concentration (MIC) in order to prevent the formation of microbial resistance [4]. But nowadays the prophylactic use of antibiotics is controversially being discussed [5], for which reason the use of inorganic components with no risk or a very low risk of resistance development is a particularly interesting approach to preventing biomaterial-associated infections.

In particular, the combination of pro-osteogenic and antimicrobial implant modifications is of great relevance in improving implant performance. In this respect the trace elements of copper (Cu) and zinc (Zn) are promising candidates.

Copper is an essential trace element that is catalytically active in various enzymes and involved in bone formation as part of lysyl oxidase. It also has pro-angiogenic effects which are potentially advantageous for implant coatings. The pro-angiogenic effect of Cu ions has already been demonstrated in various *in vitro*, *ex vivo* and *in vivo* studies [6–9]. Based on these promising first studies, interest in the use of Cu has increased significantly in recent years, and has led to the development of various Cu-containing implant types such as composites based on chitosan gels, calcium silicate bioceramics [10], and bioglasses [4, 11]. Copper has also been known for centuries for its antimicrobial properties, and consequently was included in several biomaterials with the aim of reducing microbial adhesion [11, 12].

Zinc is another trace element frequently mentioned in connection with angiogenesis [13]. In addition, both chemotactic [14] and proliferation- and differentiation-promoting effects [15, 16] were observed on osteogenic cells as a result of the presence of Zn in a concentration range of 2 to 100 μM . A local effect of accelerated bone formation could be demonstrated in rats after implantation of a Zn-releasing calcium phosphate [17].

In contrast to the above mentioned applications, where Cu and Zn were incorporated into three-dimensional bone substitutes, coatings on titanium implants offer much less mass. This raises the interesting question of whether the effects of the two trace elements will also occur for such a coating. Hence, the aim of this study was to integrate both trace elements into inorganic osteoconductive coatings and to characterize the obtained surface modifications with respect to their composition, release behavior of bioactive components, and cell-biological and antimicrobial properties. Comparing coatings with differing total amounts and ratios of Cu and Zn should allow the determination of the best overall composition. The calcium phosphate phase (CPP) of brushite was used as a carrier for the selected trace elements, to (i) provide osteoconductive surfaces and (ii) embed and retain the trace metal and enable its sustained release. The rationale behind the selection of brushite was based on the fact that it has the highest solubility of

all CPPs and is easily remodeled *in vivo*. Hence, eventual coating delamination during implant insertion would not cause any prolonged inflammatory reactions, while it could still provide the intended effects on the surrounding tissue.

The chosen method of electrochemically assisted deposition (ECAD) provides two advantages: (i) it is a comparatively cheap method, and (ii) it can deposit coatings on complex surface geometries, including hidden parts such as undercuts. This is a major benefit over other coating technologies which are line-of-sight processes and require costly equipment, such as plasma electrolytic oxidation [18], ion implantation [19], vacuum melting [20] and laser sintering [1].

2. Materials and methods

All chemicals were of analytical grade or tested for cell culture (for *in vitro* experiments) and were purchased from Sigma-Aldrich (Germany), if not stated otherwise.

2.1. Electrochemically assisted deposition

Sandblasted discs of 10 mm diameter and 2 mm height made of commercially pure titanium were produced by KLS Martin, and were of VDI 3400 specification with a surface roughness (Ra) of 3.3 μm . The discs were dual acid-etched with a mixture of HCl and H_2SO_4 , as described previously [21]. Electrochemical depositions were performed within a two-electrode assembly consisting of a fourfold-working electrode surrounded by a platinum mesh counter electrode. The samples were mounted within Teflon sample holders covering all surfaces except for the top side of the disc, and aligned in a vertical position. Cathodic polarization was performed in a galvanostatic mode controlled by a combined potentiostat/ galvanostat (PJT 120-1, Radiometer, Denmark).

The electrolyte consisted of 83.5 mM $\text{Ca}(\text{NO}_3)_2$ and 50 mM $\text{NH}_4\text{H}_2\text{PO}_4$ (pH 4.4), with or without additional $\text{Cu}(\text{NO}_3)_2$ and/or $\text{Zn}(\text{NO}_3)_2$. The total deposition time and the current density were optimized in preliminary experiments, with deposition times ranging between 15 and 60 min and current densities of 1–2 mAcm^{-2} . The first minute of deposition was carried out statically; after this period, the whole electrode assembly was rotated at 50 rpm with an amplitude of 1 cm. After deposition, the samples were rinsed twice with ultra-pure water under continuous shaking for 5 min and then dried in a gentle stream of nitrogen.

Control experiments for Cu adsorption were conducted with the highest Cu concentration used (0.5 mM $\text{Cu}(\text{NO}_3)_2$ in water) for a duration equal to the running time of a deposition process (53 min).

Table 1. Description of selected sample types: labeling, composition of electrolytes for preparation, and analysis of main components of obtained coatings.

Sample name	Composition of electrolyte [mM]				Composition of coating: mean \pm SE [μ g]			
	Ca(NO ₃) ₂	NH ₄ H ₂ PO ₄	Cu(NO ₃) ₂	Zn(NO ₃) ₂	Ca	PO ₄ ³⁻	Cu	Zn
Brushite	83.5	50	0	0	1177 \pm 58	2019 \pm 27	-0.1 \pm 1.1	-1.0 \pm 0.3
Cu01	83.5	50	0.1	0	1091 \pm 31	2152 \pm 41	4.1 \pm 0.2	0.8 \pm 1.1
Cu03	83.5	50	0.3	0	1063 \pm 41	2076 \pm 29	25.1 \pm 1.1	3.3 \pm 0.8
Zn03	83.5	50	0	0.3	1070 \pm 74	2282 \pm 49	0.14 \pm 0.07	25.7 \pm 1.4
Zn05	83.5	50	0	0.5	622 \pm 65	1132 \pm 27	0.09 \pm 0.03	56.7 \pm 4.1
Cu01Zn03	83.5	50	0.1	0.3	1419 \pm 82	3185 \pm 42	10.9 \pm 0.4	22.3 \pm 1.2
Cu01Zn05	83.5	50	0.1	0.5	978 \pm 38	2000 \pm 95	14.2 \pm 0.6	51.6 \pm 3.9
Cu03Zn03	83.5	50	0.3	0.3	1384 \pm 76	1859 \pm 41	67.8 \pm 1.0	22.4 \pm 7.1
Cu03Zn05	83.5	50	0.3	0.5	645 \pm 48	594 \pm 47	68.9 \pm 0.1	59.7 \pm 3.7

2.2. Chemical and physical characterization of the coatings

2.2.1. Chemical composition of the coatings

Determination of the calcium (Ca) and phosphate (PO₄) contents of the coatings was performed after their dissolution in concentrated nitric acid, followed by a 1:20 dilution in ultra-pure water. The respective contents of Ca, PO₄, Cu, and Zn ions were analyzed via colorimetric analysis using a Ca kit, a phosphate kit (both Greiner, Germany), a 5-Brom-PAPS kit for Zn and a DiBrPAESA kit for Cu (both Greiner Diagnostic, Germany). The Cu content was additionally analyzed with atomic absorption spectroscopy (AAS) with a 5FL (Carl Zeiss) at 460.7 nm. Solutions for AAS analysis were diluted with 0.1% potassium chloride solution. Sample labeling according to the composition of the electrolytes used and the composition of the obtained coatings is presented for selected sample types in table 1.

2.2.2. Scanning electron microscopy

The morphologies of the obtained coatings were observed by using a scanning electron microscope (SEM) XL-30 ESEM FEG (Phillips, Germany) after sputter-coating with a thin carbon layer (Baltec, Germany). Additionally, quantitative energy dispersive x-ray (EDX) analysis and EDX mapping were performed for selected coating types with a DSM 982 Gemini (Carl Zeiss, Germany) in combination with a NORAN Vantage (Noran Instruments, USA) equipped with a Si(Li) detector at 15 kV.

2.2.3. X-ray photoelectron spectroscopy

The analysis of the surface chemistry of the deposited layers was performed by x-ray photoelectron spectroscopy (XPS) in a Phi 5600 CI (Physical Electronics) system using monochromatic Al-K_α x-rays (excitation energy 1486.6 eV) with a power of 240 W at an acceleration voltage of 8 kV. The resolution of the spectrometer was about 2 eV. The evaluation of the spectra was performed with CasaXPS software (version 2.2.67). To correct the shift of the spectra due to the charging of the surfaces, the energy scale was calibrated on the basis of the Ca 2p_{3/2} peak on the

Table 2. Composition of simulated body fluid according to Tas [22].

Ions	Concentration [mM]
Na ⁺	142.0
K ⁺	5.0
Ca ²⁺	2.5
Mg ²⁺	1.5
Cl ⁻	125.0
HCO ₃ ⁻	27.0
HPO ₄ ⁻	1.0
SO ₄ ²⁻	0.5

theoretical binding energy for brushite of 347.2 eV. The quantitative elemental composition was calculated from the peak areas using element-specific sensitivity factors and the transfer function of the spectrometer.

2.2.4. XRD

The crystallographic characterization of the coatings was performed by means of x-ray diffraction (XRD) in Bragg-Brentano geometry using a Siemens D5005 x-ray diffractometer (Bruker AXS, Karlsruhe, Germany) with Cu-K_α radiation; the acceleration voltage of the x-ray tube was 40 kV and the tube current was 40 mA. The diffraction patterns were recorded in a 2 Θ range of 10–42°; the step size was 0.02° and the dwell time was set to 1 s per step.

2.3. Release of Cu and Zn ions

Release studies were carried out by incubation of the samples in 1 ml of simulated body fluid (SBF). The composition of SBF was according to Tas [22]. The respective final ion concentrations are listed in table 2 and the complete recipe is presented in table S1 in the supplement, available online at stacks.iop.org/BMM/15/025006/mmedia. The incubation was performed with or without the addition of 10% fetal bovine serum (FBS) within 48 well plates (Nunc) completely sealed with parafilm at 37 °C and 5% CO₂. The results from preliminary studies carried out over a period of nine days revealed that the highest differences in the release kinetics

between different coatings were observed within the first 3–4 days of incubation (see supplement figure S1). Therefore, release studies for the complete set of surface types were conducted for the first three medium exchanges, each being performed after 24 h.

Supernatants were collected completely, and aliquots were diluted with 0.1 M nitric acid in a ratio of 1:1 and stored in Eppendorf vials. Zn and Cu determination was performed on the same day as the medium exchange as described in 2.2.1. The calcium and phosphate contents in the solutions were collected in such a way that they were not affected by storage at 4 °C for several days, and were measured within one week of the samples being taken.

2.4. Cell biological characterization

2.4.1. Cell biological characterization with human bone marrow stromal cells

In vitro cell experiments for assessment of osteogenic induction were conducted with human bone marrow stromal cells (hMSCs), which were obtained from surplus aspirates of two bone marrow donors (donor 1: male, 20 years; donor 2: male, 25 years). The isolation of hMSCs was performed at the Dresden Bone Marrow Transplantation Center of the University Hospital Carl Gustav Carus, following the method described by Oswald *et al*; their potential for differentiation into osteogenic, chondrogenic and adipogenic lineage was verified [23]. The study had been approved by the Ethics Committee of the TU Dresden, Dresden, Germany (approval no. EK261072013, 22 August 2013). All experiments were performed in compliance with the relevant laws and institutional guidelines; written consent of the donors was obtained for the use of these aspirates for research purposes. All sample surfaces were seeded with 5000 cells cm⁻². Cultivation and analysis were performed as described in detail elsewhere [24], except for the use of 50 μM ascorbic acid phosphate instead of 300 μM ascorbic acid as osteogenic supplement.

Samples were studied as received or after pre-incubation for 3 d in serum-free SBF, as bioactive materials with the tendency to attract mineral deposition onto their surface upon contact with physiological media are known to deplete Ca from the medium and thus require treatment prior to cell seeding [25].

Cells were seeded onto samples lying in 48-well plates with 5000 cells within 500 μl of basal medium (BM), which consisted of alpha medium supplemented with 10% fetal bovine serum, 2 mM glutamate, 100 U penicillin and 100 μg ml⁻¹ streptomycin (both Biochrom AG). This refers to a density of 3.800 cells per sample surface, assuming attachment by straight sedimentation. For osteogenic induction the cells were cultivated with a differentiation medium based on BM supplemented with 50 μM ascorbic acid phosphate and 5 mM β-glycerophosphate starting at d3 after seeding.

The cell culture medium was collected at each medium exchange. The contents of released Cu and Zn ions were determined as described above. The concentration of released vascular endothelial growth factor (VEGF) was determined at day 3, day 7 and day 14, using an enzyme-linked immunosorbent assay (ELISA) kit for human VEGF (Duoset, RnD systems), in accordance with the manufacturer's instructions. VEGF release was analyzed only on the protein level in the supernatants of cultured samples, as mRNA isolation was not possible due to high nucleic acid adsorption onto calcium phosphate phases.

2.4.2. Investigations with endothelial cells

Human umbilical vein endothelial cells (HUVECs) pre-screened for sprouting activity were purchased from Promocell (Heidelberg, Germany) and used in passage 5 for all endothelial cell experiments.

In vitro 3D angiogenesis was performed according to a method initially developed by Korff and Augustin [26]. This method consists of three steps: preparation of spheroids, incorporation of spheroids into collagen gels, and stimulation with respective solutions followed by microscopic analysis. The spheroid preparation was performed one day prior to the start of the assay. Cells precultured in cell culture flasks were trypsinized when they were nearly confluent (80%–90%) and resuspended in methocel medium, resulting in 1 × 10⁴ cells per ml. The methocel medium consisted of endothelial cell BM (ECBM, Promocell) supplemented with 10% methocel stock (12 mg ml⁻¹ methyl cellulose, 100 U penicillin, 100 μg ml⁻¹ streptomycin, and 5% FBS). From this suspension, 110 μl was transferred to 96 well plates (suspension plates, Greiner Bio-One™) and cultured overnight at 37 °C at 5% CO₂. On the next day the spheroids were harvested with a 1000 μl pipette bearing tips with cut-off ends. They were collected in 50 ml Falcon tubes (two plates per tube) and centrifuged for 5 min at 1000 × g. In between, 2 ml of acidic collagen extract from rat tails (1.5 mg ml⁻¹) was mixed with 0.25 ml 10x M199 (Sigma) and incubated on ice. The pellets were loosened and the spheroids were carefully resuspended in 900 μl of the methocel-FBS medium (20% FBS and 80% methocel stock solution). Neutralization of collagen was performed by adding 100 μl of cold 0.2 M NaOH solution to the collagen solution and subsequently mixing carefully with the spheroid suspension in the ratio 1:1. From this suspension, 400 μl was added to each well of a pre-warmed 48-well plate and incubated again at 37 °C and 5% CO₂ for 30 min prior to the addition of the stimulation solutions. Next, 100 μl of each stimulation solution was added in a five-fold concentration of the final intended value. After 24 h and 48 h, sprouting activity was investigated by light microscopy. The number of sprouts per spheroid and the respective sprout length was established manually via image analysis with ImageJ version 1.51k.

Stimulation solutions were either positive controls (25 ng ml⁻¹ VEGF or 25 ng ml⁻¹ basic fibroblast growth

factor (bFGF)), negative controls (pure medium), or a solution obtained after incubation of the coated samples in 1 ml of EC medium for 24 h at 37 °C and at 5% CO₂. To exclude potentially adverse effects of the reduced calcium levels in the incubation solutions, fresh medium supplemented with Cu²⁺-ions was studied as well. Cu²⁺ concentrations were in the range of 5–500 μM, corresponding to Cu²⁺ concentrations previously published in several *in vitro* studies [7, 8].

The transwell migration assay was performed using 24-well plates (TPP) and transwell inserts (Greiner) with 8 μm pore diameter. The transwell inserts were coated with sterile acidic solution of 5 μg ml⁻¹ collagen for 1 h, washed with sterile water, and kept in water until use. The lower reservoirs of the 24 wells were filled with 750 μl of the respective stimulation solutions or extracts derived from incubation of samples in ECBM supplemented with 20% FBS. Cells were seeded into the upper reservoirs of the transwell inserts with 0.5 × 10⁴ cells in 500 μl ECBM (containing 20% FBS) and immediately moved into the respective prepared wells. The 24-well plate was incubated in a humidified atmosphere (37 °C, 5% CO₂) for 4 h. After this migration period the medium was sucked out and cells on the upper side of the membrane were removed, using a cotton swab. Phosphate buffered saline (PBS) was used to wash the transwell inserts in fresh wells, and afterwards, migrated cells on the bottom side were fixed in 1 ml of cold methanol for 20 min at 4 °C, dried for 30 min and then stained with 0.1% crystal violet for 20 min. Nine spots of the bottom side of each insert were investigated with light microscopy and the numbers of migrated cells were identified manually.

2.4.3. Antimicrobial investigations

Only those sample types that were not cytotoxic to hMSCs were subjected to microbial testing, to analyze their bactericidal activity and bacterial adhesion in terms of LIVE/DEAD staining. Sandblasted, acid-etched titanium surfaces and brushite coatings served as control. *E. coli* SM 2029 were kindly provided by the group of Elke Boschke at the Institute of Bioprocess Engineering (TU Dresden) and originally obtained from Søren Molin of the Technical University of Denmark (DTU, Lyngby). Precultures were grown overnight at 30 °C in flasks with 20 ml LB medium (Carl Roth GmbH) containing 50 μg ml⁻¹ kanamycin sulfate, at 220 rpm in a compact shaker.

From this overnight culture, 200 μl was inoculated into fresh medium and cultured until an optical density, measured in a 1 cm cuvette at 600 nm, (OD₆₀₀) of ~1 was reached (exponential phase). The bacteria suspension was filtered through a 5 μm filter (Minisart, Sartorius) to avoid the presence of bacterial clusters. Next, 50 μl of a bacterial suspension containing 1.52 × 10⁵ colony forming units (CFU) ml⁻¹, resulting in a seeding density of 1 × 10⁴ CFU cm⁻², was carefully dropped onto each sample surface. For cultivation longer than 2 h, the LB medium was diluted 1:5

with water, as suggested by Wiegand *et al* [12], to avoid excessively high growth rates in the references.

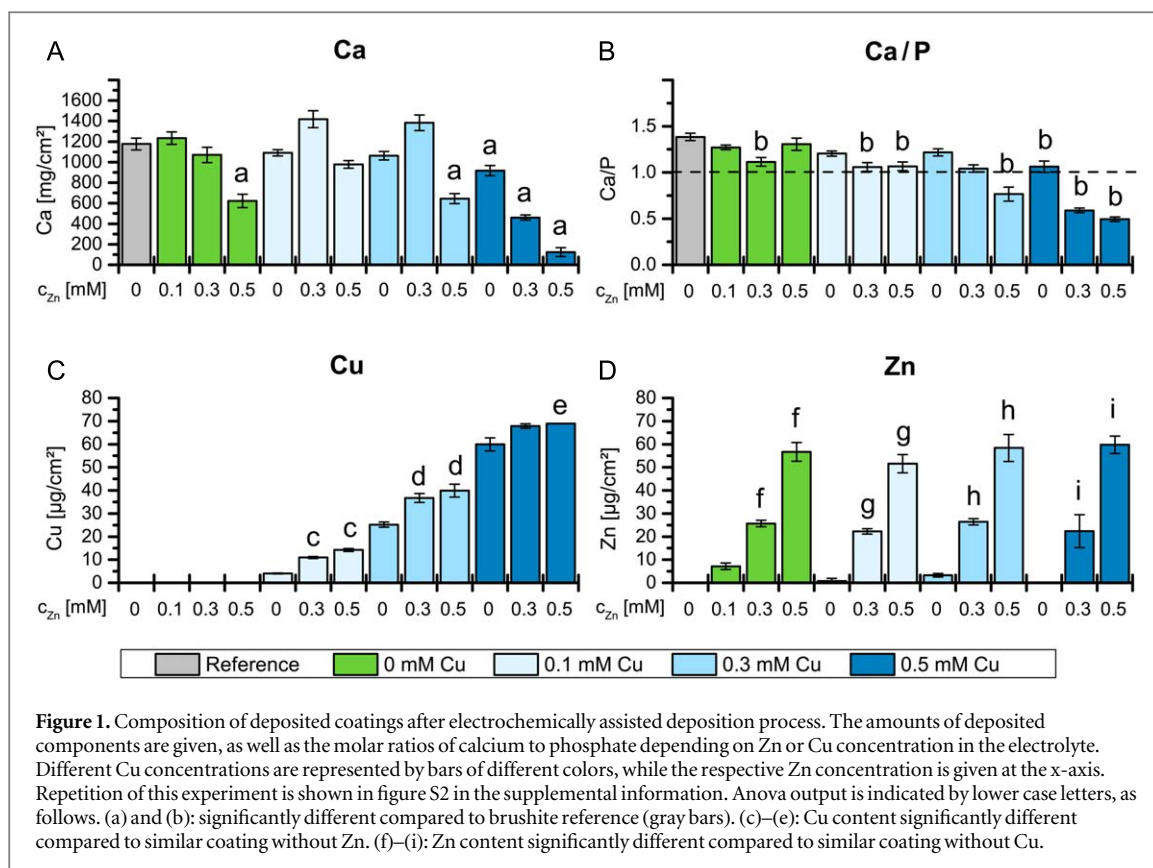
The samples were lying in central positions on the 48-well plates (suspension plates, Nunc), while all outer wells and spaces between wells were filled with sterile water to generate an atmosphere saturated with water vapor. After incubation times of 2 h and 12 h, 450 μl of fresh LB was added to each well and the plates were vigorously shaken for 5 min. Next, 300 μl of each original suspension and serial dilutions in LB medium were transferred into 96-cell culture plates (TPP) for quantification of CFU equivalents using a proliferation assay. A standard row ranging between 1 × 10⁵ CFU ml⁻¹ and 1 × 10⁷ CFU ml⁻¹ was prepared from fresh exponential culture. The plates were cultured under shaking (100 rpm) at 37 °C and OD₆₀₀ was recorded every 30 min. For further analysis, the time taken to reach a threshold of 0.1 was determined and the initial concentration of bacteria was calculated according to the calibration.

In parallel, the samples were subjected to two more washing steps in PBS. Then the LIVE/DEAD staining (Invitrogen) of the samples was performed according to the manufacturer's instructions. Staining of individual samples was conducted immediately prior to fluorescence microscopy; all other samples were stored in PBS at room temperature. Prior tests with titanium samples revealed no increase in dead cells and no substantial growth under such conditions for a storage time of up to 4 h. Pictures were taken with a cLSM 510 meta (Zeiss, Jena, Germany).

2.5. Statistical analysis

With the exception of the XPS analysis, XRD measurements and EDX mapping, all experiments were carried out in duplicate. Cell experiments with hMSCs were conducted with two donors. Biochemical analyses and antimicrobial tests were performed, each with n = 3, and cell biological experiments with n = 4. For endothelial sprouting per experimental run the spheroids were analyzed in two wells each, with n = 10. All results are shown as mean ± standard error.

Statistical analysis was performed using one-way or two-way Anova, with Levene's test for equal variances and Tukey's post hoc test with respective correction for multiple comparisons of means. Significant differences were assumed at p < 0.05. Due to the high number of respective tests, visualization of all significant differences within the figures was not possible. Instead, the output of statistical analysis was introduced into the figures for the comparison of individual means to respective controls by different letters, as denoted in the figure captions. Additional outcomes of significance tests between interesting sample coating conditions are mentioned within the text specifying respective p-values. Further, interested readers can obtain a rough visual estimation of the significance between any pairs, assuming significance when ~2x



the length of error bars would not overlap, with an exact factor of 1.86 for $p < 0.05$ for the used number of tests according to Payton *et al* [27].

3. Results

3.1. Characterization of deposited coatings

3.1.1. Coating composition

The trace elements Cu and Zn, either alone or in combination, were integrated into CPP coatings by means of ECAD under conditions favoring brushite formation. The respective coating densities of the deposited cations as well as the Ca/P ratios are shown in figure 1.

The reference coating with no added trace elements resulted in a calcium content of $1200 \mu\text{g cm}^{-2}$. The corresponding Ca/P ratio (1.32) was higher than the theoretical value for pure brushite (1.0). The addition of Zn ions to the electrolytes resulted in a linear increase of deposited Zn^{2+} ions into the CPP coating within the studied range. At the same time, a decrease in calcium and phosphate deposition was observed, visible already at 0.3 mM Zn, but more pronounced at 0.5 mM Zn. The Ca/P ratio was almost unaffected (figure 1(B)), but a linear increase in deposited Zn was determined (green bars in figure 1(D)). Between $7.2 \pm 1.4 \mu\text{g cm}^{-2}$ and $56.7 \mu\text{g} \pm 4.1 \mu\text{g cm}^{-2}$, Zn species were incorporated into the coatings, at a percentage of 0.2% (for 0.1 mM of Zn) to 1.9% (for 0.5 mM Zn) in relation to the total mass of calcium and hydrogen phosphate.

The addition of Cu ions to the electrolyte resulted in a similar linear increase of deposited amounts related to the Cu concentration in the electrolyte (figure 1(C)), reaching a comparable deposited amount of $59.6 \pm 3.9 \mu\text{g cm}^{-2}$ for the application of 0.5 mM Cu. In contrast to the above-mentioned changes in brushite deposition supplemented with Zn, no such influence was observed with respect to the absolute CPP mass or the Ca/P ratio when only Cu solution was added (figures 1(A), (B)); first of each blue bar with Zn = 0). When the two ions were added simultaneously, Cu did not affect the amount of deposited Zn (figure 1(D)), but increasing Zn concentrations slightly increased the Cu deposition (figure 1(C)). However, this effect was more pronounced at lower Cu concentrations (light blue compared to dark blue bars in figure 1(B)).

The already observed decrease in calcium (figure 1(A)) and phosphate (not shown) deposition in the presence of Zn was not further affected by up to 0.3 mM Cu, but for higher Cu concentrations (in particular, for the combination of 0.5 mM Zn and 0.5 mM Cu), a massive decrease in the Ca amount and Ca/P ratio was observed.

As brushite is known for its high capacity for the adsorption of Cu ions, the amount of Cu immobilized by simple adsorption was studied on brushite-coated reference samples exposed to 0.5 mM Cu for the same duration as the ECAD deposition process. The determined amount of immobilized Cu was $13.5 \pm 2.1 \mu\text{g cm}^{-2}$, which accounts for 22.5% of the

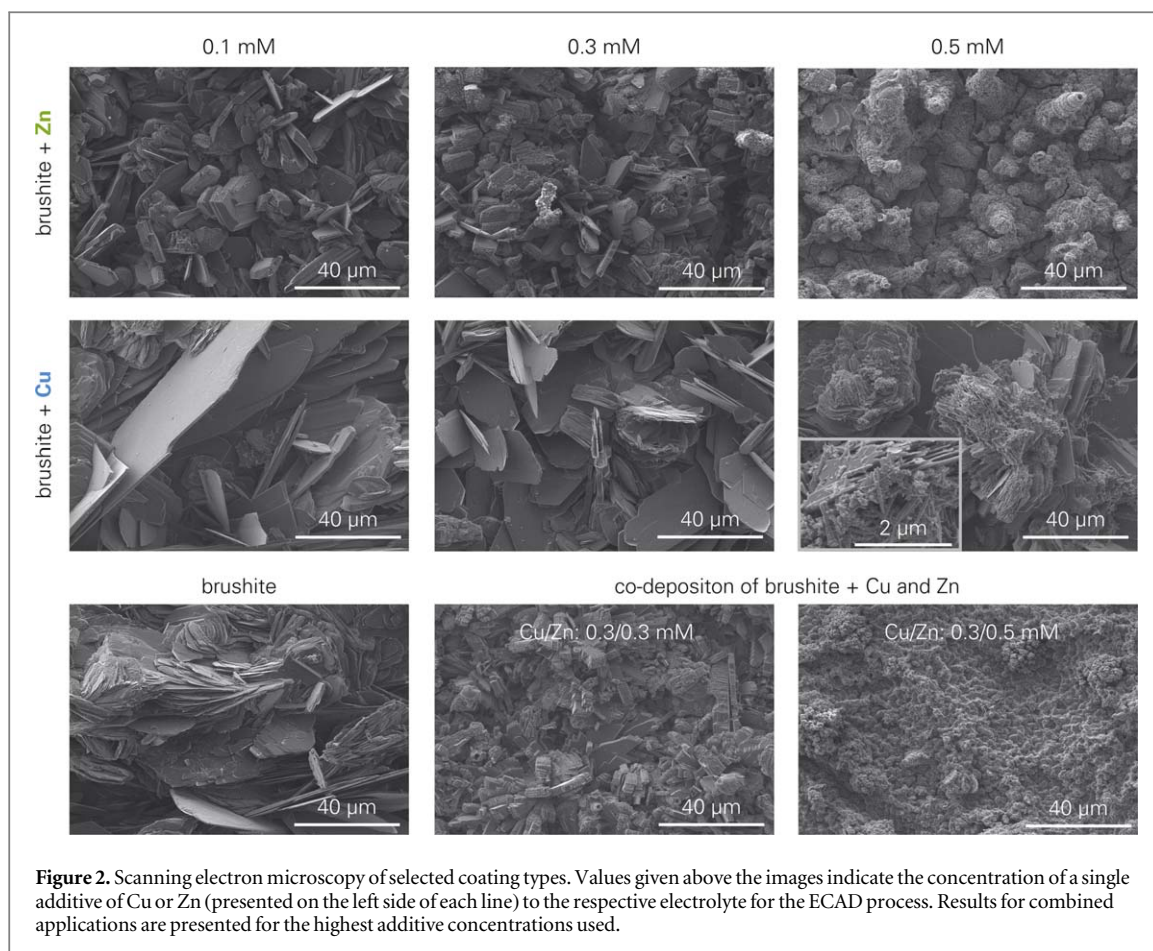


Figure 2. Scanning electron microscopy of selected coating types. Values given above the images indicate the concentration of a single additive of Cu or Zn (presented on the left side of each line) to the respective electrolyte for the ECAD process. Results for combined applications are presented for the highest additive concentrations used.

respective deposited mass obtained after the ECAD process.

3.1.2. Morphology of the deposited mineral coatings

A comparatively low concentration of 0.1 mM Zn changed the crystal morphology of deposited brushite plates from thin elongated plates to thick but small blocks. For higher Zn concentrations of up to 0.5 mM, almost no more brushite-like plates were observed (figure 2).

In contrast, the addition of Cu did not change the shape or size of the brushite plates, although with increasing Cu concentration another phase with small, dendrite-shaped particles was observed. The combination of the two ions massively reduced both the overall presence and size of brushite plates. When both ions were added to 0.5 mM, no more brushite plates were observed at all. Instead, a mixture of small irregularly-shaped mineral particles was found (figure 2).

The dendritic particles could be identified to contain only Cu species. The intensity of the Cu signal was highest in these particles and directly at the titanium (oxide) surface, while only a very slight diffuse distribution along the brushite crystals was observed (figure 3(A)). No particulate clusters (as for Cu deposition) were observed in the case of Zn immobilization at up to 0.5 mM Zn. According to EDX mapping, in coatings containing solely Zn, the respective Zn species were homogeneously distributed across the

calcium phosphate coating (see supplement figure S3), while the combination of Cu and Zn resulted in particular clusters of Cu, but homogeneous distribution of Zn (figure 3(B)).

3.1.3. XRD analysis of crystal structure

The diffraction pattern for the brushite reference clearly revealed the presence of brushite, with no other crystalline phases (figure 4). In particular, with an increasing addition of Zn ions the intensity of the brushite reflexes decreased, but the most prominent brushite reflexes were still observed. In contrast, Cu integration had only marginal impact on the diffraction patterns. Diffraction peaks which could not be assigned to CPP originated from the underlying titanium substrate, but no other crystalline phases were detected.

3.1.4. XPS analysis

In all surface types with integrated Zn and Cu, respective peaks were detected by XPS in the topmost parts of the coating surfaces with increasing intensity for increasing Cu and Zn in the electrolytes (figure 5). For all samples containing Cu, the Cu 2p peak consisted of two split spin-orbit components: Cu 2p_{1/2} at a bond energy of approximately 953 eV, and Cu 2p_{3/2} at approximately 933 eV. The 2p_{3/2} fit revealed two components with a satellite at higher binding energy. The binding energy of the first

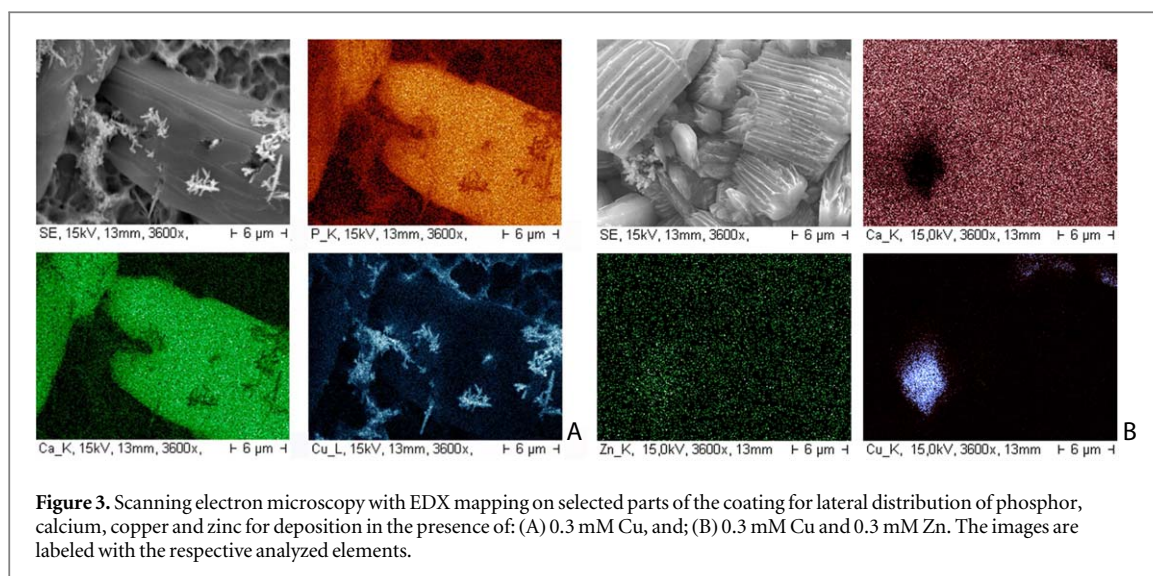


Figure 3. Scanning electron microscopy with EDX mapping on selected parts of the coating for lateral distribution of phosphor, calcium, copper and zinc for deposition in the presence of: (A) 0.3 mM Cu, and; (B) 0.3 mM Cu and 0.3 mM Zn. The images are labeled with the respective analyzed elements.

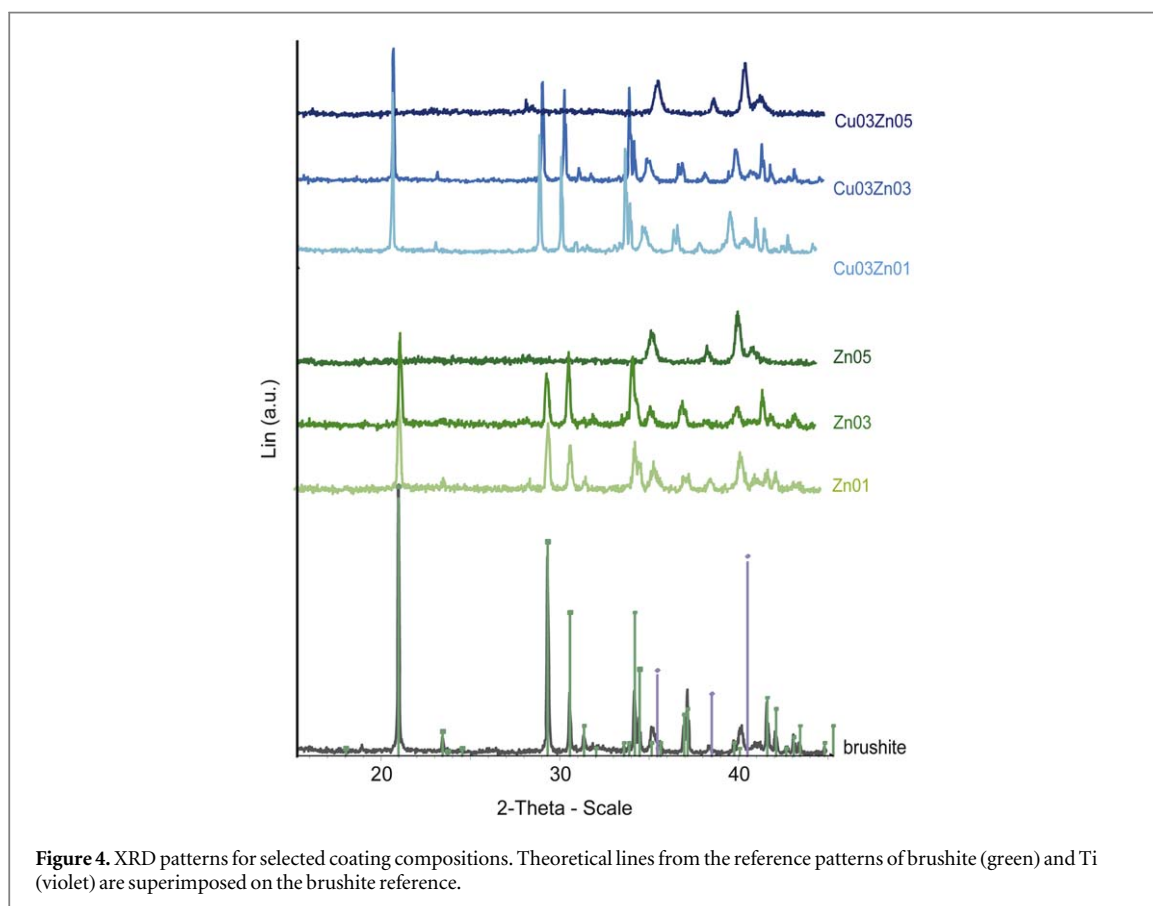


Figure 4. XRD patterns for selected coating compositions. Theoretical lines from the reference patterns of brushite (green) and Ti (violet) are superimposed on the brushite reference.

component, representing Cu(I), was 932.8 ± 0.1 eV, while that of the second component was 935.0 ± 0.3 eV, and the satellite was 944.3 ± 0.1 eV. However, when samples were exposed to γ -radiation due to a longer analysis time, the relation between the two components shifted more towards 932.8 eV. Therefore, reliable quantification of the ratio Cu(I)/Cu(II) species was not possible, but more than 70% were identified as Cu(I) in analyzing the immediately recorded spectra. For Zn only, the presence of Zn species can be derived from XPS spectra. Due to peak

deposition no further information on oxidation state or type of compound (phosphate or oxide or hydroxide) is possible.

3.1.5. Release of trace element ions

Release studies were carried out, incubating the samples in SBF with or without the addition of 10% FBS. The left part of figure 6(A) clearly shows that only minor traces of the initially deposited Cu species were released in the absence of proteins. Only for samples with the highest Cu contents (those deposited using

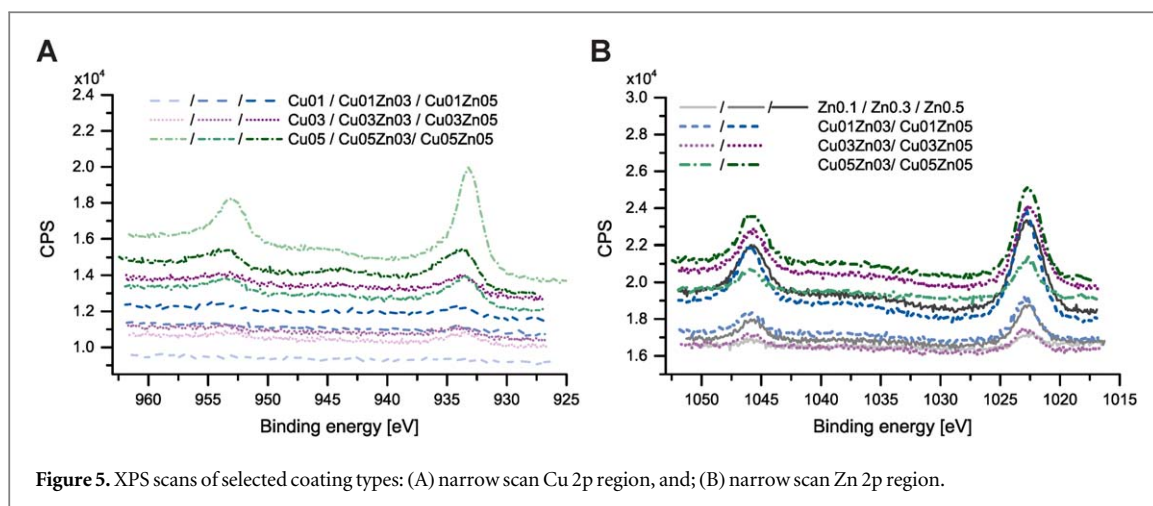


Figure 5. XPS scans of selected coating types: (A) narrow scan Cu 2p region, and; (B) narrow scan Zn 2p region.

0.5 mM Cu) was the release of Cu species significantly above the background reference. No more Cu was released in the second incubation step (24 h to 48 h), except for the combination of Cu05Zn05, where a continued release was observed after the first medium exchange. This surface type contained the lowest overall calcium content and was the only one that released calcium into this kind of incubation medium. All other surfaces states strongly depleted calcium from the used incubation medium SBF (see supplement figure S4).

In serum-containing medium the overall release (figure 6(A)) was primarily influenced by the initially immobilized Cu amount. For all surface types, the highest delivery of Cu species occurred during the first incubation step, with six times more Cu being released compared to the serum-free medium. There was also a continued release in the following incubation steps. Co-immobilized Zn showed no significant impact on the Cu release for samples with low Cu content, but for higher Cu content it reduced the Cu release.

In the absence of proteins, an equally low Zn release was likewise observed (figure 6(B), left part). Samples with high Zn (Zn05) released continuously $\sim 0.2 \mu\text{g ml}^{-1}$. The presence of Cu species in the coatings slightly increased the release, up to $0.5 \mu\text{g ml}^{-1}$ (blue curves in figure 5(B), left part); the more Cu was incorporated, the higher was the release of Zn. Incubation of the samples in the presence of proteins resulted in a concentration-dependent increase of released Zn. Compared to Cu there was no pronounced burst release, but rather a steady release over time with comparatively low amounts of $0.2 \mu\text{g ml}^{-1}$ (for 0.1 mM Zn) to $0.8 \mu\text{g ml}^{-1}$ (for 0.5 mM Zn).

Compared to the release in the cell-free systems described above, the release of Cu and Zn under cell culture conditions was significantly prolonged (figures 6(C) and (D)). Interestingly, the amounts of total released Cu and Zn species per incubation step were also significantly higher ($p < 0.05$), outweighing even the effect of cumulative release for three days (first and each subsequent uneven period) or four days

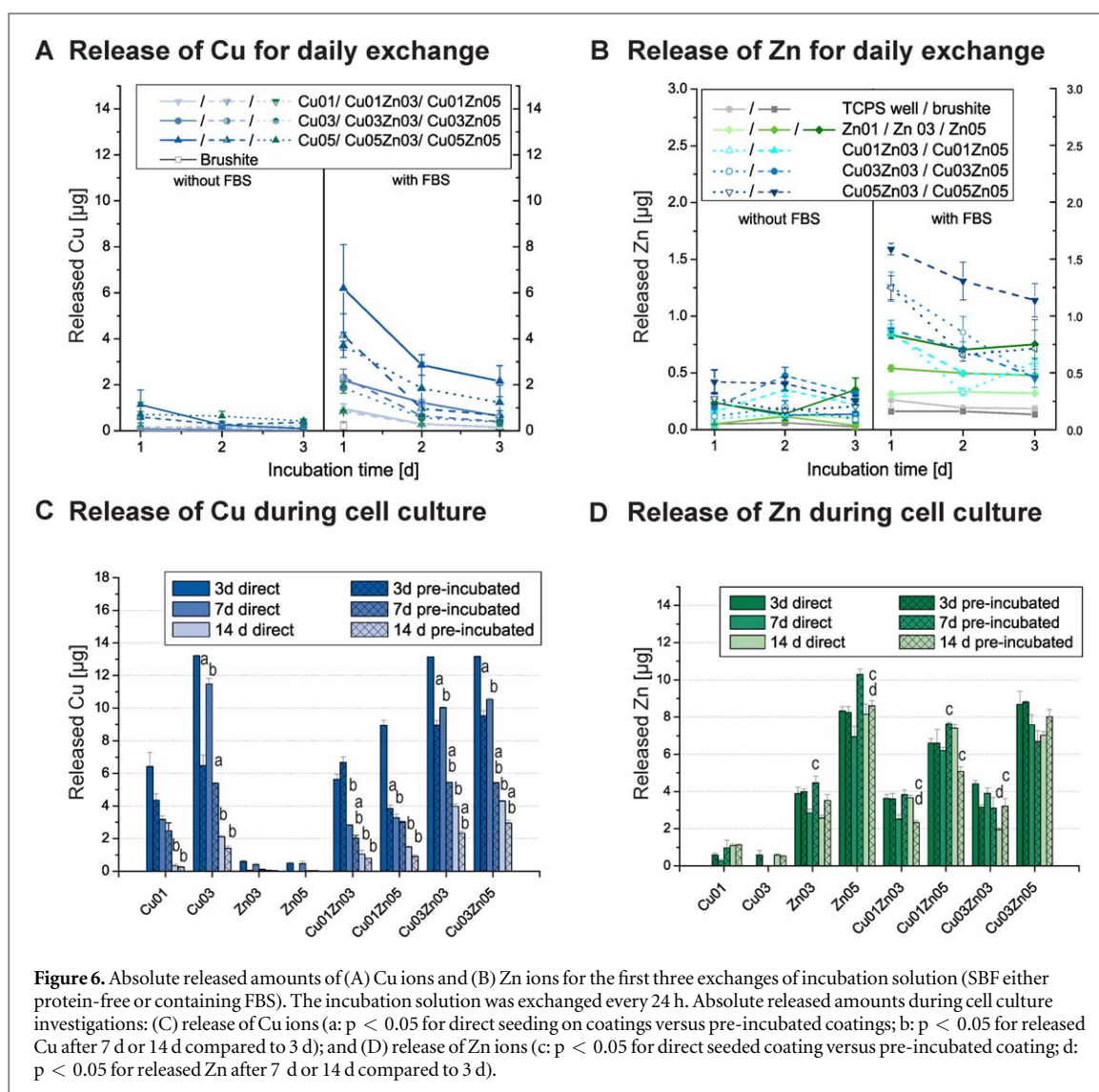
(second and each subsequent even period), respectively.

A pre-incubation of the coated samples for 3 d in protein-free SBF had no great effect on the following release patterns of Zn in the cell culture setup, with significant differences being observed only for a minor number of coating types and only for the incubation period of 7 d ($p < 0.05$ for released amounts for Zn03 and Zn05, comparing with and without pre-incubation). No marked decrease in Zn release was found in the total incubation time of 14 d. In contrast, for Cu a significant reduction of the burst release in the first two incubation steps could be achieved by such pre-incubation ($p < 0.05$). For all studied coating types, a decrease in actual release rates was observed for each exchange step.

3.2. Cell biological evaluation

3.2.1. Cell biological characterization with hMSCs

Preliminary experiments revealed that no cells adhered on samples obtained from electrolytes containing 0.5 mM Cu, either with or without additional Zn, and that cell response to all samples with low Zn content from electrolytes with 0.1 mM Zn did not differ significantly from unmodified brushite. Hence, only samples with Cu lower than 0.5 mM and Zn higher than 0.1 mM were subjected to cell-biological characterization with hMSCs. For comparison, coatings with only Cu or Zn were also analyzed. Due to known adverse consequences of direct seeding of cells onto calcium-depleting materials [25], the cell experiments were performed either with as-received coatings or after pre-incubation in protein-free SBF for three days. As shown in figures 3(A) and (B), only minor amounts of trace elements were released during such treatment, but nearly all surfaces except for Zn05 depleted calcium from the solution, in particular during the first 24 h. Pre-incubation in SBF led to dense mineral precipitation on top of the originally deposited mineral phases. Particularly for brushite and Cu01, such newly deposited mineral resembled octacalcium phosphate (OCP) crystallites and decorated

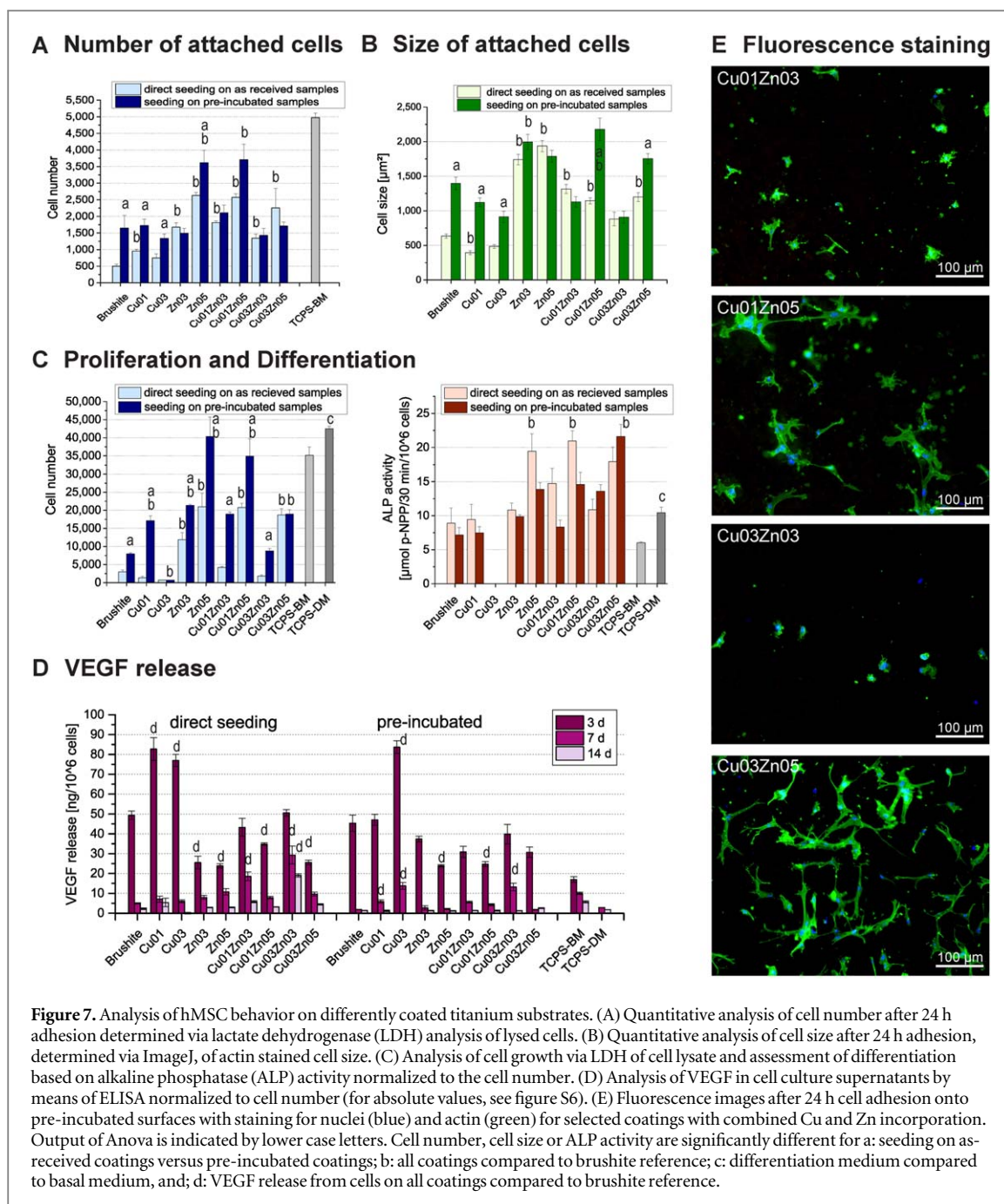


the underlying brushite plates (see supplement figure S4).

As demonstrated in figure 7(A), cell adhesion in terms of cell number clearly improved with increasing Zn incorporation into the coatings, in particular for cells seeded on as-received samples (Zn05 > Zn03 > brushite ($p < 0.01$); Cu01Zn05 > Cu01Zn03 ($p < 0.01$), and Cu03Zn05 > Cu03Zn03 ($p < 0.05$ only for direct seeding)). The opposite trend was observed for samples with increasing Cu amounts (Cu03 < Cu01; Cu03Zn03 < Cu01Zn03, and Cu03Zn05 < Cu01Zn05; $p < 0.05$ for all). Although the number of adherent cells was in general higher for pre-incubated samples (dark blue bars in figure 7(A)), similar trends were observed for as-received coatings (light blue bars in figure 7(A)). A comparatively low number of cells (~20% of the cell number in the seeding suspension) was found on top of as-received brushite coatings. In contrast, after pre-incubation in SBF, cell adhesion was markedly increased in these samples. For most of the other Cu and Zn containing sample types, except for Zn03, Cu03Zn03 and Cu03Zn05, cell adhesion was slightly improved on the pre-incubated

samples. In general, the highest cell adhesion was observed on samples coated with high Zn and low Cu content (Zn05 and Cu01Zn05), but even here, pre-incubation in SBF significantly improved cell attachment. In contrast, cell adhesion on the surrounding well surfaces was affected by the pre-treatment only for brushite and Cu01 samples (see supplement figure S5).

The trends for cell size and shape were similar to those found for cell adhesion (see figures 7(B) and (E)). The cells were largest in the presence of high Zn content, i.e., for Zn03 and Zn05, irrespective of prior pre-incubation ($p < 0.01$). Cells were elongated and had a tendency to adhere in agglomerates assembling 2–4 cells. Pre-incubation of coatings containing both Zn and Cu significantly improved cell spreading for high Zn contents (Cu01Zn05 \gg Cu01Zn03 ~ Br and Cu03Zn05 \gg Cu03Zn03 ~ Br). Direct cell seeding on all coatings combining Cu and Zn deposition resulted in cell sizes larger than on brushite or coatings with only Cu, but smaller than on coatings containing solely Zn additives ($p < 0.01$). The cells that were clearly the smallest were seen for coatings containing



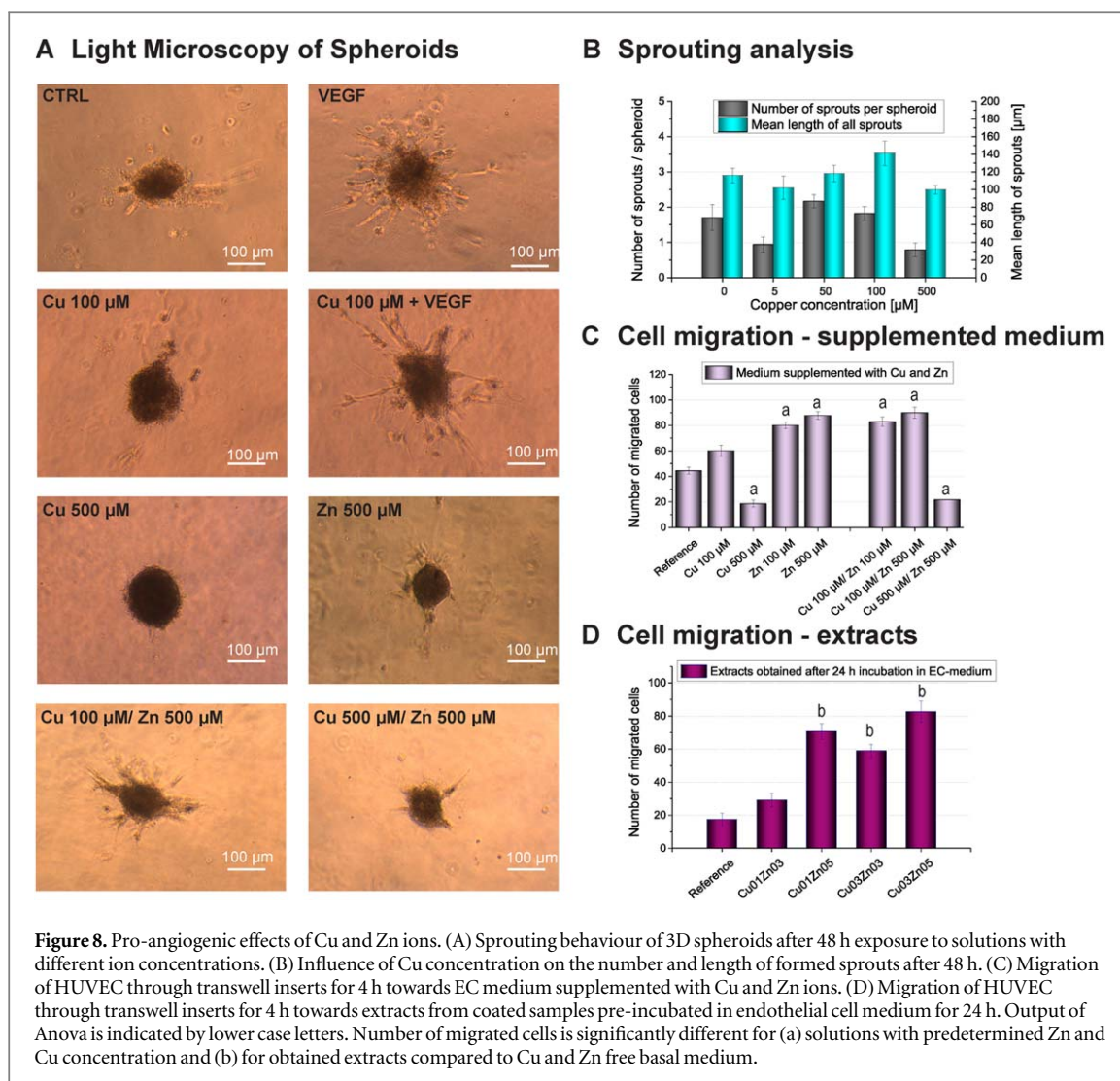
only Cu, although pre-incubation improved cell spreading to a level comparable to mixed coatings with low Zn content.

Further growth in the presence of differentiation additives (figure 7(C)) resulted in the highest overall cell numbers for samples with the highest Zn content (Zn05, Cu01Zn05) and no or low Cu content. However, in general the cell numbers after 14 days tended to reflect the situation after cell seeding (figure 7(C)) compared to figure 7(A)). For a variety of sample types, the resulting cell numbers were roughly 10 times as high as after seeding, with an overall better performance of pre-incubated samples. A markedly lower growth rate was seen for brushite, Cu01, Cu03 and Cu03Zn03, in particular when the cells were seeded on as-received samples. The most striking

difference was detected for Cu03, where no cell proliferation was seen at all.

The highest ALP activities (figure 7(C) right panel) were in general observed for samples with the highest Zn content (Zn05, Cu01Zn05, and Cu03Zn05). Interestingly, for a variety of coating types the ALP activity was comparable or even slightly higher on the as-received compared to pre-incubated samples, except for Cu03Zn03 and Cu03Zn05.

As seen in figure 7(D), the VEGF release normalized to cell number was highest for the first supernatants collected three days after cell seeding compared to all supernatants collected later ($p < 0.001$), irrespective of sample types. Interestingly, neither absolute nor relative VEGF release were influenced by the pre-incubation step (two-way



Anova, $p > 0.05$). The highest relative VEGF release was observed for brushite, Cu01, and Cu03. Increasing the Zn amount in a Zn/Cu coating while keeping the Cu constant reduced the normalized VEGF release, while increasing Cu with constant Zn resulted in a higher normalized VEGF release.

3.2.2. Impact of Cu containing coatings on endothelial cells

For *in vitro* evaluation of pro-angiogenic effects, two types of experiments were conducted with HUVECs: 3D angiogenesis starting from spheroids embedded in collagen matrix, and a transwell migration assay. Both were performed with reference solutions of known Cu and Zn ion concentrations, and with extracts from coated samples.

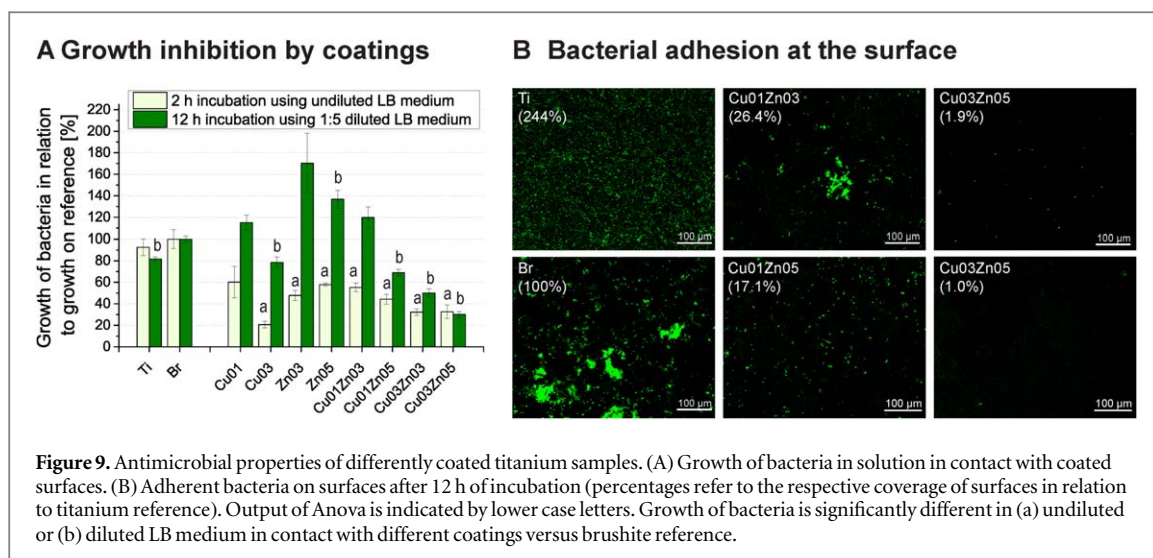
No pronounced pro-angiogenic effects were observed in the 3D angiogenesis model for extracts of any sample type. Slight sprouting could be observed in medium supplemented with an intermediate Cu concentration, high Zn, or a combination of intermediate Cu and high Zn (figure 8(A)), but with lesser numbers of sprouts compared to the response to the angiogenic factor VEGF. As Cu ions are frequently discussed to be

pro-angiogenic [2, 4, 6–9], the concentration was varied for this ion in a broader range. Although there was an intermediate increase in sprout length for 100 μM Cu after 24 h (figure S7), no more significant differences could be detected after 48 h (figure 8(B)). Also, in 2D culture no positive or negative effect was observed with up to 100 μM Cu on HUVEC proliferation, but cytotoxic effects were obvious at 500 μM (see supplement figure S9).

Clearer effects of Cu and Zn could be demonstrated in migration experiments based on gradients between upper and lower transwell inserts. The samples delivering the highest amounts of Zn resulted in the most pronounced migration, while the additional presence of Cu diminished the respective migration potential (figure 8(D)). The same trends were observed for media containing Cu and Zn ions in the range of 0–500 μM , with a high Cu concentration in the lower compartment strongly reducing migration (figure 8(C)).

3.3. Antimicrobial efficacy

The same coating types used in the hMSC experiments were further studied for antimicrobial efficacy.



First, the number of viable bacteria was assessed in suspensions after they had been in contact with the respective surfaces for 2 h or 12 h. Relative growth is presented in relation to brushite (set as 100%). After 2 h (figure 9(A)) a significantly lower number of viable bacteria was observed for all coatings, with one or both trace elements compared to titanium (Ti) or brushite references ($p < 0.05$ compared to brushite, except for Cu01). The effect was most pronounced for Cu03 ($p < 0.001$). After 12 h (figure 9(B)) of incubation the number of bacteria was again significantly lower on samples containing the higher Cu content ($p < 0.05$ for Cu03) compared to brushite or Ti, particularly when combined with additional Zn ($p < 0.01$ for Cu03Zn03 and Cu03Zn05). All other coatings were no longer effective in reducing bacterial growth in surrounding solutions.

Bacterial adhesion was investigated after incubating a bacterial suspension for 12 h on the surfaces. While a high number of viable bacteria adhered at Ti reference, a certain reduction of adherent cells was already observed for pure brushite (~40% less area covered by bacteria compared to Ti). The addition of trace elements resulted in a further decrease of bacterial coverage. Coatings with only Cu (Cu01, Cu03) and those with combinations of Zn with high Cu amounts (Cu03Zn03, Cu03Zn05) were most effective, resulting in a bacterial coverage that was less than 1% of the control (see supplement figure S10). According to LIVE/DEAD staining, nearly all bacteria on coated surfaces were dead (figure S10), while on the Ti reference almost no dead cells were found.

Interestingly, when known amounts of Zn or Cu ions were added to bacterial suspensions under otherwise identical conditions, Zn ions were more effective than Cu in inhibiting bacterial growth. Furthermore, the combination of both ions was more effective than the respective individual ions (see supplement figure S11).

4. Discussion

The overall aim of this study was to develop inorganic coatings with multifunctional properties, i.e., osteoconductive, osteoinductive, and pro-angiogenic as well as antimicrobial. To achieve this, two trace elements were integrated into calcium phosphate coatings, and the coatings with the best overall performance were identified.

4.1. Biophysical and biochemical characterization of coated samples

Electrochemically assisted deposition was used to deposit brushite coatings that contained the trace elements Cu and Zn, either alone or in combination. For electrolytes with 0.1 mM Cu, the included Cu amounts were in a similar range to those of hydroxyapatite (HAP) coatings deposited by electrochemical methods [28], with $6.5 \mu\text{g cm}^{-2}$ versus $2.4 \mu\text{g cm}^{-2}$, but the brushite coatings contained roughly 40 times more calcium phosphate. This indicates that the Cu deposition occurred independently of the CPP deposition, an assumption supported by the separate Cu containing species observed within EDX scans and by the fact that the calculated Ca masses and Ca/P ratios were unaffected by different Cu concentrations. XPS analysis showed the deposited Cu species to consist mainly of Cu(I) species, most probably of cuprous oxide (CuO), which is similar to those found in HAP coatings [28]. In summary, Cu deposition depended mainly on the concentration of added Cu and on parameters influencing reduction processes during electrochemical polarization, such as time and current density. The necessary conditions for the reduction of Cu^{2+} ions were achieved directly at the Ti surface and on top of the brushite plates, probably by nascent hydrogen.

Completely different behavior was observed for the addition of Zinc ions. Although the ion diameter of Zn^{2+} (0.74 pm) is comparable to that of Cu^{2+} (0.73 pm),

with both being significantly smaller than the Ca^{2+} ion (0.97 pm), the presence of Zn ions strongly affected the brushite deposition. Hence, it can be assumed that Zn was partially integrated into the brushite lattice. However, as no changes in the XRD peaks were observed, we conclude that Zn exchanged places with Ca in the lattice but only in the outer layers of the crystals, thereby inhibiting further growth in a concentration-dependent manner and increasing the deposition of amorphous CPP. This is consistent with the homogeneous Zn distribution seen in EDX mapping. According to Heidmann *et al* [29] and Izaki *et al* [30], Zn could also be deposited as ZnO, ZnOH, or $\text{Zn}_3(\text{PO}_4)_2$ under the applied conditions. Although XPS studies demonstrated only the presence of Zn, determination of the exact chemical nature was not possible due to similar peak positions of the respective references.

4.2. Ion release

The release behavior of trace element ions is of high importance for the effect of surface modifications on the surrounding tissue after implantation. It can be studied under conditions as close as possible to physiological ones with respect to protein and ion content in the incubation media, as this can significantly influence the release. In this study we used 10% FBS which, although different from the *in vivo* situation, is the usual supplement for cell studies. To allow for comparison with the results of other published studies we also used a protein-free incubation medium (SBF). Most of the coatings studied here depleted calcium from SBF, but in the presence of proteins this was the case only for brushite and Cu01, the coating most similar to brushite.

The presence of proteins clearly showed a tremendous impact on the release kinetics of both ionic species. Without proteins, nearly no Cu and only low Zn amounts were released. This is unsurprising, as Cu and Zn phosphates have low solubility and the presence of 1.0 mM phosphate in the incubation medium should prevent their dissolution, while the more readily soluble hydroxides or oxides might be reprecipitated as phosphates. Accordingly, soluble Cu and Zn species were found only in the first change of incubation medium, and this only for the highest Cu and Zn amounts.

For Cu and Zn, specific transport proteins are present in the serum: ceruloplasmin and albumin for Cu, and albumin and α 2-macroglobulin for Zn [31]. Under physiological conditions only 2.6% of the albumin is loaded with Zn. Albumin has one high affinity binding site for Zn, two of medium affinity, and 15 low affinity, so it is unsurprising that in preliminary tests we could not find any saturation for up to $15 \mu\text{g ml}^{-1}$ of released Zn using different FBS supplementations (5%, 10%, or 15%). Hence, the comparatively continuous release of Zn in the presence of serum proteins is probably due to slow exchange processes, and the

amounts released depend primarily on the initially deposited amount. The slightly higher release of Zn in coatings with a high Cu content might be explained by a lower binding affinity of CPP for Zn in the presence of competing Cu ions. Cu05Zn05 was the only coating that released Ca into the incubation medium, resulting in a dissolution rather than a restructuring of the respective (amorphous) CPP and consequently the highest release of both ions.

In contrast to the continuous release of Zn, a burst-like release was observed for Cu-containing samples that was irrespective of the initial Cu content, or the presence or absence of additional Zn. This effect was probably due to the high percentage of separate CuO phases seen as agglomerates or dendrites. As these fractions are not associated with the coated CPP, the serum proteins in the incubation medium could easily complex the Cu ions. Proteins can form stable complexes with Cu^{1+} ions [32, 33] and with Cu^{2+} ions [34]. The exact oxidation state of the released Cu was not specified as the used Cu assay cannot distinguish between them.

Under cell culture conditions (figure 6(B)), higher amounts of both ions were released per incubation interval compared to release studies in SBF (figure 6(A)), even taking into account the 3–4 times higher concentrations due to the longer incubation intervals. As the same FBS batch was used and preliminary tests without cells had shown no difference for SBF and cell culture medium when both contained 10% FBS, it is possible that cellular activity leads to some additional remobilization of deposited trace element ions. The co-deposition of Cu and Zn had no effect on the release patterns compared to references containing only Cu or Zn. However, samples with high Cu content (from electrolytes containing 0.5 mM Cu) were not studied in this experiment due to strong cytotoxicity.

One interesting point should be highlighted. The pre-incubation in serum-free SBF—which was required for some coating types to improve cell adhesion—markedly reduced the burst release of Cu in the first incubation step (see figure 6(B)), in particular for the highest Cu content and irrespective of additional Zn. As only traces of Cu were delivered in this step, it is expected that Cu ions might be embedded into newly formed CPPs.

4.3. Cell biological effects

The trace element ions were incorporated to trigger different biological effects. In addition to the potential antimicrobial effects of both trace element ions (discussed in 4.4), Zn was added to attract progenitor cells through chemotaxis and to increase osteogenic induction. Cu on the other hand was integrated into the coatings for its known pro-angiogenic effects [6–8, 10, 35].

Cell adhesion and differentiation were clearly enhanced in the presence of Zn-containing coatings, both with and without additionally immobilized Cu species (figures 7(A)–(E)). The effects of incorporated Zn corresponded quite well with previously reported effects [14, 16, 17]. The most pronounced effects on cell adhesion (figures 7(A) and (B)) and on growth (figure 7(C)) and differentiation (figure 7(D)) in our experiments were observed for all coatings with the highest Zn concentration (0.5 mM Zn supplementation leading to $\sim 60 \mu\text{g cm}^{-2}$ Zn in coatings, corresponding to 1.9% related to coating mass). This Zn content was nearly identical to the effective dose of 1.2% Zn in calcium phosphate cements reported by Ito *et al* [36] using MC3T3 cells. However, it has to be kept in mind that the efficacy *in vivo* might be different, as the authors found a maximum stimulation of bone regeneration in healthy rabbits for a fourfold lower Zn content of 0.3% (w/w) using the same scaffolds [17].

The presence of Cu provoked neither detrimental nor beneficial effects on hMSC provided the Cu content was equal to or below $\sim 10 \mu\text{g cm}^{-2}$ (corresponding to 0.03% of the calcium phosphate coating mass, obtained for electrolyte supplementation with 0.1 mM). Although the released Cu amounts for all analyzed coatings resulted in sub-toxic concentrations ($4\text{--}6 \mu\text{g ml}^{-1}$, corresponding to $\sim 20\text{--}90 \mu\text{M}$) in the total volume, the local concentration directly at the surface was apparently too high to allow for the survival of attached cells. The *in vivo* situation might differ, as the initially formed blood clot is expected to limit cell contact to the surface and to affect the interaction of the coating with soluble proteins. The importance of such local effects was also reflected by an increased adhesion of cells to the multiwell surface in comparison to the sample surface (see supplement, figure S5).

Aside from the direct effects of both trace elements on cellular behavior, the indirect influence due to changes in the calcium phosphate phase must also be considered. Depending on the actual composition and crystallinity of the CPP, a certain dissolution and reprecipitation of calcium phosphates will occur, which might compromise *in vitro* cell adhesion, growth, and differentiation, as was observed for other bioactive surfaces [37]. Pre-incubation in serum-free SBF was applied to alleviate such phenomena. Accordingly, the brushite reference and coatings with high amounts of crystalline brushite (Cu01, Cu03) performed significantly better after this step. Other coatings with markedly increased cell adhesion and growth after pre-incubation were Zn05 and Cu01Zn05. Here, pre-incubation did not change total Zn release but recrystallization processes were obviously beneficial for these surface types, too. The above-mentioned decrease of Cu burst release was definitely advantageous for all Cu-containing samples. Under applied incubation conditions (maintaining the physiological pH by a sufficiently carbonate-buffered SBF in 5%

CO_2), conversion into more stable calcium phosphate phases such as octacalcium phosphate or apatite-like carbonated phases can be expected [38, 39]. This is consistent with observed CPP precipitations resembling OCP crystallites, in particular for brushite and coatings containing pure Cu or Zn. Phases containing both trace elements were also covered by a dense, newly deposited CPP layer, but it consisted of small globular particles instead (figure S4). On all surfaces a dense and uniform layer with no separate phases was found. With respect to Cu release, this implies that a firm embedding of Cu oxide species by the newly formed dense mineral deposits is able to modify the release behavior. Substitution of Ca by Cu ions within the mineral lattice is rather improbable due to the large differences in ion radii. In contrast to Cu, the Zn species are already strongly embedded within original mineral phases, and consequently pre-incubation had no great effect on the release kinetics.

In summary, the best overall osteogenic stimulation of hMSC was found for the combination of high Zn and low Cu content (Zn05, Cu01Zn05). The combination of high Cu and high Zn (Cu03Zn05) was also promising, with comparatively good cell attachment and spreading in combination with a high ALP activity.

Although the pro-angiogenic effects of released Cu have frequently been demonstrated *in vivo* and *in vitro* [6–8, 10, 35], here the growth of endothelial cells in monoculture was affected neither in the 2D nor the 3D angiogenesis models. These outcomes are consistent with previous experiments combining the pro-angiogenic factors VEGF and bFGF with Cu ions, both with and without additional heparin (see supplement, figure S8). There, a significant increase in sprouting activity was observed only for growth factor supplementation, while the addition of Cu did not result in any significant changes. While the pro-angiogenic effect of bFGF was not impaired, the VEGF-induced stimulation (number of sprouts) even decreased in the presence of Cu (see supplement, figure S7).

This raises the question of whether it is possible to evaluate the pro-angiogenic effect of Cu using *in vitro* endothelial cell monoculture models. The *in vitro* effect of Cu is reported to be based on stabilizing the hypoxia inducible factor 1 α (HIF-1 α), which in turn leads to an up-regulation of pro-angiogenic genes, with VEGF among them [40]. But in endothelial cells, self-activation induced by HIF-1 α up-regulates VEGF by a factor of only 1.5 [41], and indeed a significant up-regulation was demonstrated mainly for other cells such as keratinocytes [9] and hepatocytes [42]. More complex *in vitro* and *ex vivo* models such as the chick embryo chorioallantoic membrane (CAM) [35, 43], zebra fish embryos [16] or co-culture models with fibroblasts [10] or hMSC [44] showed a much clearer impact of Cu on angiogenesis. It can be deduced that the effect of Cu is based on the response of the cells residing in vascularized tissues such as osteoblasts,

fibroblasts and/or immune cells, rather than on the direct response of the endothelial cells.

Accordingly, a significant increase of normalized and absolute VEGF secretion was shown for hMSC for coatings containing only Cu, while Zn, either alone or in combination with Cu, resulted in a reduction of VEGF secretion (see figure S6 for absolute values). However, it is not only the relative but also the absolute VEGF secretion that would be important for stimulation of adjacent endothelial cells in co-culture models or *in vivo*. In this respect, all coatings with high Zn content (Zn05, Cu01Zn05, Cu03Zn05) were promising, with Cu01Zn05 showing the highest overall VEGF secretion within the first three days, while Cu03Zn05 provoked a comparably high VEGF secretion over the entire cell culture period of 14 days.

Interestingly, released Zn had a direct stimulatory effect on endothelial cells in the migration experiment and increased motility. This corresponded with the slightly increased sprouting activity observed within 3D-angiogenesis model.

4.4. Antimicrobial efficacy

Both trace elements have been used in biomedical applications due to their well-known antimicrobial effects, but amounts of Cu that were still subtoxic to human cells could not completely eradicate bacteria. This is in agreement with previous findings for Cu integrated into bioglass or Cu/Ti oxide composite layers [31].

We conclude that there is no therapeutic window for Cu that simultaneously provides both biocidal properties and biocompatibility to human cells. However, we agree with Burghardt *et al* [31] that it might be promising to develop coatings with an initial burst release of Cu, thus providing increased biocidal activity shortly after implantation and a prolonged delivery of very low amounts. Barralet *et al* [6] demonstrated pro-angiogenic effects exclusively for scaffolds releasing low amounts of Cu. Thus, a prolonged Cu delivery of high amounts of Cu is not recommended. The additional integration of Zn was not only favorable for the stimulation of hMSC adhesion and differentiation, as discussed above, but also beneficial to antimicrobial activity. The most promising bacterial reduction—both in solution and on the surface—was found for the coating with the highest Cu and highest Zn contents (Cu03Zn05).

It is generally advised to combine different antimicrobial compounds to efficiently combat bacterial contamination and particularly biofilms [45], so potentiated effects through the incorporation of both ions are unsurprising. The most relevant modes of antimicrobial activity appear to be the generation of reactive oxygen species via a Fenton reaction, and the high tendency of proteins to form complexes with Cu ions [46] that compromise their biological activity, but these are probably also the reason for the cytotoxicity

of higher amounts of Cu. The bacterial susceptibility to Zn, on the other hand, seems to be based on an extracellular competition between Zn^{2+} and essential Mn^{2+} binding to specific proteins [44]. The mode of action of both trace elements thus differs, and specific ion efflux pumps would be required to develop resistance.

E. coli was used as a model strain in the current study to permit comparison to multiple other biomaterials with antimicrobial effects [47–50]. It was also identified in peri-implant lesions and postulated to play a significant role of enterics in the context of peri-implantitis [51]. However, for more specific characterization of the interplay between incorporated Cu and Zn under conditions of the oral cavity, multispecies models [52–54] or direct *in situ* tests [55] would be recommended. Likewise, for orthopaedic implants, specific fine tuning of Cu and Zn incorporation would require additional experiments with *S. aureus* and *S. epidermidis*.

5. Conclusions

We demonstrated a comparatively easy method of depositing osteoconductive CPP coatings on titanium surfaces that have additional multi-functionality, namely the stimulation of angiogenesis, the attraction and stimulation of bone-forming cells, and the exertion of at least inhibitory effects on bacteria in close vicinity to the implant. Despite the slightly better biocompatibility of surfaces with lower Cu content, the combination with the highest Zn and Cu contents (Cu03Zn05) is considered to be the most favorable due to the low bacterial adhesion and strong bactericidal effect directly at the surface. As the Cu content can be easily tuned without compromising the capacity of the coatings for Zn incorporation, the final decision for the optimal coating composition should be further clarified by appropriate *in vivo* investigations.

Acknowledgments

The authors would like to thank the German Research Foundation (Grant no: WO 1903/2-1 and MO 1768/2-1) for providing financial support to this project.

ORCID iDs

C Wolf-Brandstetter  <https://orcid.org/0000-0001-9509-6145>

References

- [1] Safi I N, Hussein B M A, Al Shammari A M and Tawfiq T A 2019 Implementation and characterization of coating pure titanium dental implant with sintered β -TCP by using Nd: YAG laser *The Saudi Dental Journal* (<https://doi.org/10.1016/j.sdentj.2018.12.004>)

- [2] Raphael J, Holodniy M, Goodman S B and Heilshorn S C 2016 Multifunctional coatings to simultaneously promote osseointegration and prevent infection of orthopaedic implants *Biomaterials* **84** 301–14
- [3] Jennings J A, Beenken K E, Skinner R A, Meeker D G, Smeltzer M S, Haggard W O and Troxel K S 2016 Antibiotic-loaded phosphatidylcholine inhibits staphylococcal bone infection *World Journal of Orthopedics* **7** 467
- [4] Ryan E J, Ryan A J, González-Vázquez A, Philippart A, Ciraldo F E, Hobbs C, Nicolosi V, Boccaccini A R, Kearney C J and O'Brien F J 2019 Collagen scaffolds functionalised with copper-eluting bioactive glass reduce infection and enhance osteogenesis and angiogenesis both *in vitro* and *in vivo* *Biomaterials* **197** 405–16
- [5] Kühn K-D, Lieb E and Berberich C 2016 PMMA bone cement: what is the role of local antibiotics *Maitrise Orthopedique* **243** 1–15 (https://www.heraeus.com/media/media/hme/doc_hme/press_hme/2016_3/ALAC_Artikel_MO_EN.pdf)
- [6] Barralet J, Gbureck U, Habibovic P, Vorndran E, Gerard C and Doillon C J 2009 Angiogenesis in calcium phosphate scaffolds by inorganic copper ion release *Tissue Eng. Part A* **15** 1601–9
- [7] Gérard C, Bordeleau L-J, Barralet J and Doillon C J 2010 The stimulation of angiogenesis and collagen deposition by copper *Biomaterials* **31** 824–31
- [8] Giavaresi G, Torricelli P, Fornasari P, Giardino R, Barbucci R and Leone G 2005 Blood vessel formation after soft-tissue implantation of hyaluronan-based hydrogel supplemented with copper ions *Biomaterials* **26** 3001–8
- [9] Sen C K, Khanna S, Venojarvi M, Trikha P, Ellison E C, Hunt T K and Roy S 2002 Copper-induced vascular endothelial growth factor expression and wound healing *Am. J. Physiol.: Heart Circ. Physiol.* **282** H1821–7
- [10] Kong N, Lin K, Li H and Chang J 2014 Synergy effects of copper and silicon ions on stimulation of vascularization by copper-doped calcium silicate *J. Mater. Chem. B* **2** 1100–10
- [11] Bari A, Bloise N, Fiorilli S, Novajra G, Vallet-Regí M, Bruni G, Torres-Pardo A, González-Calbet J M, Visai L and Vitale-Brovarone C 2017 Copper-containing mesoporous bioactive glass nanoparticles as multifunctional agent for bone regeneration *Acta Biomater.* **55** 493–504
- [12] Wiegand C, Völpel A, Ewald A, Remesch M, Kuever J, Bauer J, Griesheim S, Hauser C, Thielmann J and Tonndorf-Martini S 2018 Critical physiological factors influencing the outcome of antimicrobial testing according to ISO22196/JIS Z 2801 *PLoS One* **13** e0194339
- [13] Shian S-G, Kao Y-R, Wu F Y-H and Wu C-W 2003 Inhibition of invasion and angiogenesis by zinc-chelating agent disulfiram *Mol. Pharmacol.* **64** 1076–84
- [14] Kanno S, Anuradha C and Hirano S 2001 Chemotactic responses of osteoblastic MC3T3-E1 cells toward zinc chloride *Biol. Trace Elem. Res.* **83** 49–55
- [15] Du R L, Chang J, Ni S Y, Zhai W Y and Wang J Y 2006 Characterization and *in vitro* bioactivity of zinc-containing bioactive glass and glass-ceramics *J. Biomater. Appl.* **20** 341–50
- [16] Seo H-J, Cho Y-E, Kim T, Shin H-I and Kwun I-S 2010 Zinc may increase bone formation through stimulating cell proliferation, alkaline phosphatase activity and collagen synthesis in osteoblastic MC3T3-E1 cells *Nutr. Res. Pract.* **4** 356–61
- [17] Kawamura H, Ito A, Miyakawa S, Layrolle P, Ojima K, Ichinose N and Tateishi T 2000 Stimulatory effect of zinc-releasing calcium phosphate implant on bone formation in rabbit femora *Journal of Biomedical Materials Research: An Official Journal of The Society for Biomaterials, The Japanese Society for Biomaterials, and The Australian Society for Biomaterials and the Korean Society for Biomaterials* **50** 184–90
- [18] Rokosz K, Hryniewicz T, Kacalak W, Tandecka K, Raen S, Gaiaschi S, Chapon P, Malorny W, Matýsek D and Dudek Ł 2018 Characterization of porous phosphate coatings enriched with calcium, magnesium, zinc and copper created on CP titanium grade 2 by plasma electrolytic oxidation *Metals* **8** 411
- [19] Yu Y, Jin G, Xue Y, Wang D, Liu X and Sun J 2017 Multifunctions of dual Zn/Mg ion co-implanted titanium on osteogenesis, angiogenesis and bacteria inhibition for dental implants *Acta Biomater.* **49** 590–603
- [20] Liu R, Memarzadeh K, Chang B, Zhang Y, Ma Z, Allaker R P, Ren L and Yang K 2016 Antibacterial effect of copper-bearing titanium alloy (Ti-Cu) against *Streptococcus mutans* and *Porphyromonas gingivalis* *Sci. Rep.* **6** 29985
- [21] Wolf-Brandstetter C, Hänchen V, Schwenzer B, Aeckerle N, Schliephake H and Scharnweber D 2016 Application of lateral and distance spacers in an oligonucleotide based immobilization system for bioactive molecules onto titanium implants *ACS Appl. Mater. Interfaces* **8** 3755–64
- [22] Jalota S, Bhaduri S and Tas A 2006 Effect of carbonate content and buffer type on calcium phosphate formation in SBF solutions *J. Mater. Sci., Mater. Med.* **17** 697–707
- [23] Oswald J, Boxberger S, Jørgensen B, Feldmann S, Ehninger G, Bornhäuser M and Werner C 2004 Mesenchymal stem cells can be differentiated into endothelial cells *in vitro* *Stem Cells* **22** 377–84
- [24] Wolf-Brandstetter C, Hempel U, Clyens S, Gandhi A, Korostynska O, Oswald S, Tofail S, Theilgaard N, Wiesmann H-P and Scharnweber D 2012 The impact of heat treatment on interactions of contact-poled biphasic calcium phosphates with proteins and cells *Acta Biomater.* **8** 3468–77
- [25] Wolf-Brandstetter C, Roessler S, Storch S, Hempel U, Gbureck U, Nies B, Bierbaum S and Scharnweber D 2013 Physicochemical and cell biological characterization of PMMA bone cements modified with additives to increase bioactivity *J. Biomed. Mater. Res. B* **101B** 599–609
- [26] Korff T and Augustin H G 1998 Integration of endothelial cells in multicellular spheroids prevents apoptosis and induces differentiation *J. Cell Biol.* **143** 1341–52
- [27] Payton M E, Greenstone M H and Schenker N 2003 Overlapping confidence intervals or standard error intervals: what do they mean in terms of statistical significance? *J. Insect Sci.* **3**
- [28] Wolf-Brandstetter C, Oswald S, Bierbaum S, Wiesmann H P and Scharnweber D 2014 Influence of pulse ratio on codeposition of copper species with calcium phosphate coatings on titanium by means of electrochemically assisted deposition *J. Biomed. Mater. Res., Part B* **102** 160–72
- [29] Heidmann I and Calmano W 2008 Removal of Zn (II), Cu (II), Ni (II), Ag (I) and Cr (VI) present in aqueous solutions by aluminium electrocoagulation *J. Hazard. Mater.* **152** 934–41
- [30] Izaki M and Omi T 1996 Transparent zinc oxide films prepared by electrochemical reaction *Appl. Phys. Lett.* **68** 2439–40
- [31] Burghardt I, Lüthen F, Prinz C, Kreikemeyer B, Zietz C, Neumann H-G and Rychly J 2015 A dual function of copper in designing regenerative implants *Biomaterials* **44** 36–44
- [32] Huang T, Long M and Huo B 2010 Competitive binding to cuprous ions of protein and BCA in the bicinchoninic acid protein assay *Open Biomed. Eng. J.* **4** 271
- [33] Park G Y, Lee J Y, Himes R A, Thomas G S, Blackburn N J and Karlin K D 2014 Copper-peptide complex structure and reactivity when found in conserved his-xaa-his sequences *JACS* **136** 12532–5
- [34] Klotz I M and Curme H G 1948 The thermodynamics of metallo-protein combinations. Copper with bovine serum albumin *JACS* **70** 939–43
- [35] Mroczek-Sosnowska N, Sawosz E, Vadalasetty K P, Łukasiewicz M, Niemieć J, Wierzbicki M, Kutwin M, Jaworski S and Chwalibog A 2015 Nanoparticles of copper stimulate angiogenesis at systemic and molecular level *Int. J. Mol. Sci.* **16** 4838–49
- [36] Chandraleka S, Ramya K, Chandramohan G, Dhanasekaran D, Priyadharshini A and Panneerselvam A 2014 Antimicrobial mechanism of copper (II) 1, 10-phenanthroline and 2, 2'-bipyridyl complex on bacterial and fungal pathogens *J. Saudi Chem. Soc.* **18** 953–62
- [37] Wolf-Brandstetter C, Roessler S, Storch S, Hempel U, Gbureck U, Nies B, Bierbaum S and Scharnweber D 2013 Physicochemical and cell biological characterization of PMMA bone cements modified with additives to increase bioactivity *J. Biomed. Mater. Res., Part B* **101** 599–609

- [38] Lu X and Leng Y 2005 Theoretical analysis of calcium phosphate precipitation in simulated body fluid *Biomaterials* **26** 1097–108
- [39] Mandel S and Tas A C 2010 Brushite ($\text{CaHPO}_4 \cdot 2\text{H}_2\text{O}$) to octacalcium phosphate ($\text{Ca}_8(\text{HPO}_4)_2(\text{PO}_4)_4 \cdot 5\text{H}_2\text{O}$) transformation in DMEM solutions at 36.5 °C *Mater. Sci. Eng., C* **30** 245–54
- [40] Feng W, Ye F, Xue W, Zhou Z and Kang Y J 2009 Copper regulation of hypoxia-inducible factor-1 activity *Mol. Pharmacol.* **75** 174–82
- [41] Manalo D J, Rowan A, Lavoie T, Natarajan L, Kelly B D, Shui Q Y, Garcia J G and Semenza G L 2005 Transcriptional regulation of vascular endothelial cell responses to hypoxia by HIF-1 *Blood* **105** 659–69
- [42] Martin F, Linden T, Katschinski D M, Oehme F, Flamme I, Mukhopadhyay C K, Eckhardt K, Tröger J, Barth S and Camenisch G 2005 Copper-dependent activation of hypoxia-inducible factor (HIF)-1: implications for ceruloplasmin regulation *Blood* **105** 4613–9
- [43] Gupte A and Mumper R J 2009 Elevated copper and oxidative stress in cancer cells as a target for cancer treatment *Cancer Treat. Rev.* **35** 32–46
- [44] McDevitt C A, Ogunniyi A D, Valkov E, Lawrence M C, Kobe B, McEwan A G and Paton J C 2011 A molecular mechanism for bacterial susceptibility to zinc *PLoS Pathog.* **7** e1002357
- [45] Campoccia D, Montanaro L and Arciola C R 2013 A review of the biomaterials technologies for infection-resistant surfaces *Biomaterials* **34** 8533–54
- [46] Stevenson J, Barwinska-Sendra A, Tarrant E and Waldron K 2013 Mechanism of action and applications of the antimicrobial properties of copper *Microbial Pathogens and Strategies for Combating Them: Science, Technology and Education* ed A Méndez-Vilas (Badajoz, Spain: Formatex Research Center) pp 468–79
- [47] Fisher L E, Hook A L, Ashraf W, Yousef A, Barrett D A, Scurr D J, Chen X, Smith E F, Fay M and Parmenter C D 2015 Biomaterial modification of urinary catheters with antimicrobials to give long-term broadspectrum antibiofilm activity *J. Controlled Release* **202** 57–64
- [48] Gouveia W, Jorge T, Martins S, Meireles M, Carolino M, Cruz C, Almeida T and Araújo M 2014 Toxicity of ionic liquids prepared from biomaterials *Chemosphere* **104** 51–6
- [49] Kumar R, Oves M, Almeelbi T, Al-Makishah N H and Barakat M 2017 Hybrid chitosan/polyaniline-polypropylene biomaterial for enhanced adsorption and antimicrobial activity *J. Colloid Interface Sci.* **490** 488–96
- [50] Moreira J, Ponmozhi J, Campos J, Miranda J and Mergulhão F 2015 Micro- and macro-flow systems to study *Escherichia coli* adhesion to biomedical materials *Chem. Eng. Sci.* **126** 440–5
- [51] Leonhardt Å, Renvert S and Dahlén G 1999 Microbial findings at failing implants *Clin. Oral. Implan. Res.* **10** 339–45
- [52] Guggenheim B, Giertsen E, Schüpbach P and Shapiro S 2001 Validation of an in vitro biofilm model of supragingival plaque *J. Dent. Res.* **80** 363–70
- [53] Kommerein N, Doll K, Stumpp N S and Stiesch M 2018 Development and characterization of an oral multispecies biofilm implant flow chamber model *PLoS One* **13** e0196967
- [54] Vilarrasa J, Delgado L M, Galofré M, Álvarez G, Violant D, Manero J M, Blanc V, Gil F J and Nart J 2018 In vitro evaluation of a multispecies oral biofilm over antibacterial coated titanium surfaces *J. Mater. Sci., Mater. Med.* **29** 164
- [55] Tawakoli P, Al-Ahmad A, Hoth-Hannig W, Hannig M and Hannig C 2013 Comparison of different live/dead stainings for detection and quantification of adherent microorganisms in the initial oral biofilm *Clin. Oral Investigations* **17** 841–50